Evaporation and combustion of multicomponent fuel droplets

Tomoaki Kitano, Jun Nishio, Ryoichi Kurose*, Satoru Komori

Department of Mechanical Engineering and Science, and Advanced Research Institute of Fluid Science and Engineering, Kyoto University, Kyoto daigaku-Katsura, Nishikyo-ku, Kyoto 615–8540, Japan

Abstract

The effects of difference in fuel components on the droplet evaporation and combustion are numerically investigated. Jet-A is used as liquid fuel, and one (n-decane)-, two (n-decane and 1,2,4-trimethyl-benzene)- and three (n-dodecane, iso-octane and toluene)-component fuels are used as the surrogate fuels of Jet-A. The results show that the evaporation of the three-component surrogate fuel becomes faster and slower than those of the one- and two-component surrogate fuels in the initial and subsequent evaporating periods, respectively. The differences in the gas temperature evolution among these three different surrogate fuels are remarkable right after the ignition, but become small with time.

Key words: Droplet evaporation, Combustion, High pressure, Multicomponent fuel, Numerical simulation

1. Introduction

Spray combustion is utilized in many industrial devises such as gas turbine engines and diesel engines. Recently, the spray combustion behavior has been studied by means of two- or three-dimensional direct numerical simulations (DNSs) (e.g., [1–18]) or large-eddy simulations (LESs) (e.g., [19–23]). However, the mechanism of spray combustion has not been fully understood yet.

Evaporation of fuel droplets is one of the most important factors in the spray combustion and strongly depends on the fuel components. Therefore it is important to take

*Corresponding author. fax: +81 75 383 3610.
Email address: kurose@mech.kyoto-u.ac.jp (Ryoichi Kurose)

the fuel components into account in order to precisely predict the combustion phenomena by numerical simulations. Daïf et al. [24] performed an experiment using a single and a few droplets of multicomponent fuel composed of n-decane and n-heptane, and compared the evaporation rate and droplet temperature with the results calculated by the evaporation model of Abramzon and Sirignano [25]. They showed that the evaporation model extended to multicomponent droplet evaporation in forced convection gave good results on the droplet radius regression and the droplet surface temperature evolution. For multiple droplets, Le Clercq and Bellan [26] performed a direct numerical simulation of a mixing layer laden with evaporating droplets of multicompoent fuel (i.e., gasoline and diesel) and compared the results with those of the one-component fuel. They pointed out that the one-component fuel could be substituted for the multicomponent fuel, but it caused the increased evaporation time.

Very recently, Borghesi et al. [17] performed a direct numerical simulation of n-heptane spray autoignition in a turbulent flow. They found that higher turbulence intensity in the carrier gas enhanced the droplet evaporation and air/fuel mixing, and then ignition. In this study, however, only a one-component fuel was used and the effects of fuel component was not discussed.

The purpose of this study is to numerically investigate the effects of difference in fuel components on the droplet evaporation and combustion. Jet-A is used as liquid fuel, and a one-component fuel (n-decane), a two-component fuel (n-decane and 1,2,4-trimethyl-benzene) and a three-component fuel (n-dodecane, iso-octane and toluene) are used as the surrogate fuels of Jet-A. For the calculation of the reaction, 113 species and 891 reactions for the one- and two-component fuels and 273 species and 2322 reactions for the three-component fuel are considered, respectively. The ambient pressure ranges from 0.1 MPa to 1.0 MPa, and the evaporation model for the multicomponent fuels in the high pressure conditions is extended based on our previous work (Kitano et al. [27]).

2. Numerical Simulation

2.1. Numerical method

The set of governing equations of the carrier gas and dispersed droplets phases and the numerical procedure are described in our previous paper [27]. To remove grid resolution dependency, source terms for gas phase are calculated for cells surrounding each droplet by using distance function from droplet position [17].

The evaporation model used in this study is mainly based on a non-equilibrium Langmuir-Knudsen evaporation model [28, 29] and validated by comparing with the experiment by Nomura and Ujiie [30]. Multicomponent evaporation is taken into account using the discrete multicomponent method [31, 32], in which each component individually evaporates according to its volatility. It is assumed that the temperature and composition are uniform inside the droplet. It is also assumed that the entire evaporation rate of multicomponent fuel is calculated in analogous way to that of a one-component fuel.

The entire evaporation rate of multicomponent fuel, $\dot{m}_d$, is expressed as

$$\dot{m}_d = -\frac{m_d}{\tau_d}\left(\frac{Sh}{3Sc}\right)\ln(1+B_M), \tag{1}$$

where

$$B_M = \frac{\sum_k Y_{V,s,k} - \sum_k Y_{V,k}}{1-\sum_k Y_{V,s,k}}, \tag{2}$$

$$\tau_d = \frac{\rho_d d^2}{18\mu}, \tag{3}$$

$$Sc = \frac{\mu}{\rho\sum_k Y_{V,k}D_k}, \qquad Sh = 2 + 0.552 Re_{sl}^{1/2} Sc^{1/3}. \tag{4}$$

Here Sc is the averaged Schmit number, Sh the averaged Sherwood number, B_M the mass transfer number, τ_d the particle response time, $Y_{V,k}$ the vapor mass fraction of kth species, ρ_d the density of liquid fuel, d the droplet diameter, μ the viscosity of gas and Re_{sl} the slip Reynolds number, respectively. $Y_{V,s,k}$ is the surface vapor mass fraction of kth species calculated as

$$Y_{V,s,k} = \frac{X_{V,s,k}}{X_{V,s,k} + (1-X_{V,s,k})\overline{W}/W_{V,k}}, \tag{5}$$

$$X_{V,s,k} = X_{k,d}\frac{P_{sat,k}}{P} - \left(\frac{2L_k}{d}\right)\beta. \tag{6}$$

Here $X_{V,s,k}$ is the surface vapor mole fraction of kth species, $X_{k,d}$ the mole fraction of fuel in the liquid phase, P the ambient pressure, $\overline{W}$ the averaged mole weight and $W_{V,k}$ the mole weight of kth species, respectively. $P_{sat,k}$ is the saturated vapor pressure calculated by Sato's empirical equation [33] as

$$P_{sat,k}^{0.119} = 11.9T^{0.119} + C. \tag{7}$$

Here the unit of $P_{sat,k}$ is [mmHg] and C is the empirical constant calculated from values in a standard condition. L_k and β are the Knudsen layer thickness of kth species and the non-dimensional constant calculated as

$$L_k = \frac{\mu\left\{2\pi T_d(R/W_{V,k})\right\}^{1/2}}{ScP}, \tag{8}$$

$$\beta = -\left(\frac{\rho_d Pr}{8\mu}\right)\frac{d}{dt}d^2, \tag{9}$$

respectively. Here T_d is the droplet temperature, Pr the Prandtl number and R the universal gas constant, respectively.

The evaporation rate of kth species, $\dot{m}_{d,k}$, is calculated as

$$\dot{m}_{d,k} = \epsilon_k \dot{m}_d. \tag{10}$$

Here ϵ_k is the non-dimensional partial evaporation rate calculated as follows [31, 32]. The conservation equation of each component around the droplet leads another form of $\dot{m}_d$ which is expressed by using k-th species properties as

$$\dot{m}_d = -\frac{m_d}{\tau_d}\left(\frac{Sh_k}{3Sc_k}\right)\ln(1+B_{M,k}), \tag{11}$$

where

$$B_{M,k} = \frac{Y_{V,s,k} - Y_{V,k}}{\epsilon_k - Y_{V,s,k}}, \tag{12}$$

$$Sc_k = \frac{\mu}{\rho D_k}, \qquad Sh_k = 2 + 0.552Re_{sl}^{1/2}Sc_k^{1/3}. \tag{13}$$

Here $B_{M,k}$ is the mass transfer number of kth species, Sh_k the Sherwood number of kth species and Sc_k the Schmit number of kth species. From Eqs. (1) and (11), the relationship between B_M and $B_{M,k}$ is written as

$$B_{M,k} = (1+B_M)^{\eta_k} - 1, \qquad \eta_k = \frac{ShSc_k}{Sh_k Sc}. \tag{14}$$

From Eqs. (2), (12) and (14) with the assumption of $\eta_k = 1$ (unity Lewis number assumption), ϵ_k is calculated as

$$\epsilon_k = Y_{V,s,k} + (Y_{V,s,k} - Y_{V,k}) \frac{1 - \sum Y_{V,s,k}}{\sum Y_{V,s,k} - \sum Y_{V,k}}. \tag{15}$$

2.2. Combustion reaction mechanism

Jet-A is used as liquid fuel, and a one-component fuel (n-decane ($C_{10}H_{22}$)), a two-component fuel (n-decane ($C_{10}H_{22}$) 82.6 wt%, 1,2,4-trimethyl-benzene (C_9H_{12}) 17.4 wt%) [34] and a three-component fuel (n-dodecane ($C_{12}H_{26}$) 45 wt%, iso-octane (C_8H_{18}) 29 wt%, toluene (C_7H_8) 26 wt%) [35–37] are used as the surrogate fuels of Jet-A. For the calculation of reaction, 113 species and 891 reactions for the one- and two-component fuels [34] and 273 species and 2322 reactions for the three-component fuel [35–37] are considered, respectively.

2.3. Computational details

Fig. 1 shows the schematic of the computational domain. The computational domain is a cube 4.8 mm on a side and divided into 48 uniform computational grid points in each direction. This grid resolution is determined based on our previous study [27].

The computations are performed for the evaporation of a single fuel droplet and for the evaporation/combustion reaction of multiple fuel droplets. Initially, the single fuel droplet and multiple fuel droplets are allocated at the center of the computational domain and in the central region as a spherical shape with 2 mm diameter, respectively. The equivalence ratio in the central region is 2.0 for multiple fuel droplets. The initial droplet diameters are set to 1.33 mm for a single fuel droplet and 7.5, 15 μm for multiple fuel droplets. These droplet sizes are decided to compare with the experiments [24] and to meet the requirement associate with the grid size from the point of view of numerical accuracy, respectively (the grid spacing needs to be roughly 10 times larger than the droplet size [10]). The initial gas and droplet temperature are 1500 K and 300 K, respectively.

Table 1 lists the numerical conditions performed for the evaporation/combustion reaction of the multiple fuel droplets. The ambient pressure, P, is set to 0.1 MPa and

1.0 MPa. In order to investigate the effects of combustion reaction, the computations are carried out for different mediums of the ambient gas (i.e., nitrogen and air). Physical properties of each component are listed in Table 2. In this table, the latent heat, L_V, is the value at normal boiling point and the heat capacity, c_p, and density, ρ, are the values in a standard condition.

The Variable-coefficient ODE solver (VODE) [38] is applied to the calculation of the detailed reaction mechanisms described above. The values of the droplet density, ρ_d, and the specific heat of the droplet, $c_{p,d}$, are calculated by the curve fit data from the NIST web book [39], and the other thermophysical properties and transport coefficients under various pressures are obtained from CHEMKIN [40, 41].

The CPU time is 6,400 h for a heaviest case (Case 9) on SGI Altlx ICE8200EX using Intel X5560 (using 64 cores).

3. Results and discussion

3.1. Evaporation of a single fuel droplet without combustion reaction

In this section, the present evaporation model is validated by comparing with the experiment by Daïf et al. [24]. In this experiment [24], a *n*-decane ($C_{10}H_{22}$)/*n*-heptane (C_7H_{16}) multicomponent droplet is suspended in a hot air flow whose average velocity is 3.1 m/s and temperature is 348 K. The initial droplet diameter is 1.33 mm and the initial droplet temperature is equal to the room temperature. In the calculation, the composition of the droplet is changed. Namely, the compositions of the droplets of Cases A and D, Case B and Case C are *n*-decane/*n*-heptane (26%/74%), *n*-heptane (100%) and *n*-decane (100%), receptively. In addition, the physical properties of individual components are considered in Case A, whereas the droplet is treated as a one-component fuel in which averaged physical properties are used in Case D.

Fig. 2 shows the comparison of the predicted time variations of the squared droplet diameter with the experiment [24]. It is shown that the decreasing rate in the experiment [24] changes at around t=7.0 s. This is because *n*-heptane mainly evaporates before at around t=7.0 s and *n*-decane mainly evaporates after that. It is found that Case A correctly predicts this change of decreasing rate, and the curve trend agrees

well with the experiment [24]. On the other hand, Case D cannot predict this change of decreasing rate especially after at around t=7.0 s, and Cases B and C fail to predict the experiment [24]. Therefore, the model in Case A is employed for the computations in the following sections.

3.2. Evaporation of multiple fuel droplets without combustion reaction

Fig. 3 shows the time variations of normalized masses of gas and liquid fuels in nitrogen for P=0.1 MPa and d_0=15.0 μm for one-, two- and three-component fuels (Cases 1-3). In these cases, the evaporation and pyrolysis occur without combustion reaction. It is found that the evaporation rate in Case 3 (three-component fuel) is higher and lower than those in the other cases before and after at t=0.1 ms, respectively. This is due to the fact that compared to n-decane and 1,2,4-trimethyl-benzene, iso-octane and toluene included in the three-component fuel have higher volatilities, whereas n-dodecane included in the three-component fuel has lower volatility. In all cases, the amount of gas fuel decreases after around 0.5 ms. This is because the pyrolysis rate overcomes the evaporation rate. Fig. 4 shows the radial distributions of spatial-averaged gas temperatures in nitrogen for P=0.1 MPa and d_0=15.0 μm for one-, two- and three-component fuels (Cases 1-3). In all cases, the gas temperatures decrease with time due to the latent heat of evaporation and heat transferred into the droplets. The gas temperature in Case 3 (three-component fuel) is found to be lower than those in the other cases at earlier periods of t=0.125 and 0.200 ms. This is due to the facts that evaporation in Case 3 (three-component fuel) is faster than those in the other cases as shown in Fig. 3, and that iso-octane and toluene of three-component fuel have larger latent heat than that of n-decane.

3.3. Evaporation of multiple fuel droplets with combustion reaction

Fig. 5 shows the typical behavior of droplet evaporation and combustion, namely the instantaneous distributions of gas temperature, and mass fractions of O_2, CO, CO_2 and OH in air for P=0.1 MPa and d_0=15.0 μm at t=0.125 ms, t=0.200 ms and t=0.400 ms for a one-component fuel (Case 4). It is observed that the gas temperature increases

with time by combustion and O_2 is consumed, and that the combustion products and radicals such as CO, CO_2 and OH are generated.

Fig. 6 shows the time variations of normalized masses of gas and liquid fuels in air for one-, two- and three-component fuels for (a) P=0.1 MPa and d_0=15.0 μm (Cases 4-6), (b) P=1.0 MPa and d_0=15.0 μm (Cases 7-9) and (c) P=0.1 MPa and d_0=7.5 μm (Cases 10-12). In Fig. 6 (a), it is found that the evaporation rate in Case 6 (three-component fuel) is higher and lower than those in Cases 4 (one-component fuel) and 5 (two-component fuel) before and after at t=0.1 ms, respectively. This is due to the same reason as mentioned earlier. Namely, compared to n-decane and 1,2,4-trimethyl-benzene, iso-octane and toluene included in the three-component fuel have higher volatilities, whereas n-dodecane included in the three-component fuel has lower volatility.

The comparisons of Fig. 6 (a) with Figs. (b) and (c) show that the differences in the evaporation rate observed between the three-component fuel and the one- and two-component fuels for P=0.1 MPa and d_0=15.0 μm still exist for P=1.0 MPa, but disappear for d_0=7.5 μm. This suggests that the effects of the droplet composition on the evaporation rate do not depend on the ambient pressure very much, but the effects become remarkable with increasing the droplet size.

Fig. 7 shows the radial distributions of spatial-averaged gas temperatures in air for one-, two- and three-component fuels for (a) P=0.1 MPa and d_0=15.0 μm (Cases 4-6), (b) P=1.0 MPa and d_0=15.0 μm (Cases 7-9) and (c) P=0.1 MPa and d_0=7.5 μm (Cases 10-12). For all pressure and initial-droplet-diameter conditions, the differences in the gas temperature among the one-, two- and three-component fuels are observed to be marked initially, and become small with time. Also, the trends of the differences in the gas temperature among one-, two- and three-component fuels are found to be different for each pressure and initial-droplet-diameter condition. In Fig.7 (b), the gas temperature in Case 9 (three-component fuel) is higher than those in Cases 7 (one-component fuel) and 8 (two-component fuel) at t=0.125 ms. This is due to the fact that the evaporation rate in Case 9 (three-component fuel) is higher than those in Cases 7 (one-component fuel) and 8 (two-component fuel) as shown in Fig. 6 (b), and

therefore the higher concentration of the evaporated fuel accelerates the combustion reaction.

On the other hand, in Fig. 7 (a), the gas temperatures not only in Case 6 (three-component fuel) but also in Case 4 (one-component fuel) indicate the higher values than that in Case 5 (two-component fuel) at t=0.125 ms. This is because the ignition delay time of the one-component fuel is shorter than that of the two-component fuel. The reason why the gas temperature of the one-component fuel is not higher than that of the two-component fuel in the case of P=1.0 MPa (see Fig. 7 (b)) is considered to be that since the ignition delay time becomes much shorter due to the higher combustion reaction rate, the difference in the ignition delay time does not affect the difference in the time variation of the gas temperature very much.

It is found in Fig. 7 (c) that the trend of the differences in the gas temperature among the one-, two- and three-component fuels is different from those in the other pressure and initial-droplet-diameter conditions. Namely, the gas temperatures in Case 10 (one-component fuel) and Case 12 (three-component fuel) are highest and lowest at t=0.125 ms, respectively. This is due to the fact that in the cases of small droplets, the time variation of the gas temperature mainly depends on the ignition delay time because evaporation of the small droplets becomes fast and there exists little difference in the evaporation rate as shown in Fig. 6 (c).

4. Conclusions

In this study, the effects of difference in fuel components on droplet evaporation and combustion were numerically investigated. Jet-A is used as liquid fuel, and one (n-decane)-, two (n-decane and 1,2,4-trimethyl-benzene)- and three (n-dodecane, iso-octane and toluene)-component fuels are used as the surrogate fuels of Jet-A. The main results obtained in this study can be summarized as follows.

1. The multicomponent droplet evaporation model which considers each component's physical properties such as boiling point and saturated vapor pressure individually precisely predicts the change of decreasing rate of droplet diameter, compared to the evaporation model which uses the averaged values of the

components.

2. Evaporation of the three-component surrogate fuel of Jet-A becomes faster and slower than those of the one- and two-component surrogate fuels in the initial and subsequent evaporating periods, respectively. This is due to the fact that compared to n-decane and 1,2,4-trimethyl-benzene, iso-octane and toluene included in the three-component surrogate fuel have higher volatilities, whereas n-dodecane included in the three-component fuel has lower volatility.
3. Differences in the gas temperature evolution among three different surrogate fuels of Jet-A are remarkable right after the ignition, but they become small with time.

Acknowledgments

The authors are grateful to Dr. Hiroaki Watanabe of Central Research Institute of Electric Power Industry (CRIEPI) for many useful discussions. This research was partially supported by "Strategic Programs for Innovative Research (SPIRE) - Field No. 4: Industrial Innovations" from MEXT (Ministry of Education, Culture, Sports, Science, and Technology).

References

[1] Cooper CS, Laurendeau NM. Quantitative measurements of nitric oxide in high-pressure (2-5 atm), swirl-stabilized spray flames via laser-induced fluorescence. Combust Flame 2000;123:175-188.

[2] Nakamura M, Akamatsu F, Kurose R, Katsuki M. Combustion mechanism of liquid fuel spray in gaseous flame. Phys Fluids 2005;17:123301.

[3] Domingo P, Vervisch L, Réveillon J. DNS analysis of partially premixed combustion in spray and gaseous turbulent flame-bases stabilized in hot air. Combust Flame 2005;140:172-195.

[4] Réveillon J, Vervisch L. Analysis of weakly turbulent dilute-spray flames and spray combustion regimes. J Fluid Mech 2005;537:317-347.

[5] Watanabe H, Kurose R, Hwang S-M, Akamatsu F. Characteristics of flamelets in spray flames formed in a laminar counterflow. Combust Flame 2007;148:234-248.

[6] Watanabe H, Kurose R, Komori S, Pitsch H. Effects of radiation on spray flame characteristics and soot formation. Combust Flame 2008;152:2-13.

[7] Baba Y, Kurose R. Analysis and flamelet modeling for spray combustion. J Fluid Mech 2008;612:45-79.

[8] Neophytou A, Mastorakos E, Cant RS. DNS of spark ignition and edge flame propagation in turbulent droplet-laden mixing layers. Combust Flame 2010;157:1071-1086.

[9] Hayashi J, Watanabe H, Kurose R, Akamatsu F. Effects of fuel droplet size on soot formation in spray flames formed in a laminar counterflow. Combust Flame 2011;158:2559-2568.

[10] Luo K, Pitsch H, Pai MG, Desjardins O. Direct numerical simulations and analysis of three-dimensional n-heptane spray flames in a model swirl combustor. Proc Combust Inst 2011;33:2143-2152.

[11] Fujita A, Watanabe H, Kurose R, Komori S. Two-dimensional direct numerical simulation of spray flames - Part 1: Effects of equivalence ratio, fuel droplet size and radiation, and validity of flamelet model. Fuel 2013;104:515-525.

[12] Kitano T, Nakatani T, Kurose R, Komori S. Two-dimensional direct numerical simulation of spray flames - Part 2: Effects of ambient pressure and lift, and validity of flamelet model. Fuel 2013;104:526-535.

[13] Hagihara K, Yamashita H, Yamamoto K. Numerical study on influence of size and number density of droplet on spray combustion mode. J Combust Soc Japan 2009;51:343-353 (In Japanese).

[14] Schroll P, Wandel AP, Cant RS, Mastorakos E. Direct numerical simulations of autoignition in turbulent two-phase flows. Proc Combust Inst 2009;32:2275-2282.

[15] Neophytou A, Mastorakos E, Cant RS. Complex chemistry simulations of spark ignition in turbulent sprays. Proc Combust Inst 2011;33:2135-2142.

[16] Botero ML, Huang Y, Zhu DL, Molina A, Law CK. Synergistic combustion of droplets of ethanol, diesel and biodiesel mixtures. Fuel 2012;94:342-347.

[17] Borghesi G, Mastorakos E, Cant RS. Complex chemistry DNS of n-heptane spray autoignition at high pressure and intermediate temperature conditions. Combust

Flame 2013;160:1254-1275.

[18] Wang H, Luo K, Fan J. Effects of turbulent intensity and droplet diameter on spray combustion using direct numerical simulation. Fuel 2014;121:311-318.

[19] Moin P, Apte SV. Large-eddy simulation of realistic gas turbine combustors. AIAA J 2006;44:698-708.

[20] Boileau M, Pascaud S, Riber E, Cuenot B, Gicquel LYM, Poinsot TJ, Cazalens M. Investigation of two-fluid methods for large eddy simulation of spray combustion in gas turbines. Flow Turb Combust 2008;80:291-321.

[21] Patel N, Menon S. Simulation of spray-turbulence-flame interactions in a lean direct injection combustor. Combust Flame 2008;153:228-257.

[22] Ihme M, Pitsch H. Modeling of radiation and nitric oxide formation in turbulent non-premixed flames using a flamelet/progress variable formulation. Phys Fluids 2008;20:055110.

[23] Moriai H, Kurose R, Watanabe H, Yano Y, Akamatsu F, Komori S. Large-eddy simulation of turbulent spray combustion in a subscale aircraft jet engine combustor - Predictions of NO and soot concentrations -. J Eng Gas Turbines Power 2013;135:091503.

[24] Daïf A, Bouaziz M, Chesneau X, Chérif AA. Comparison of multicomponent fuel droplet vaporization experiments in forced convection with the Sirignano model. Exp Therm Fluid Sci 1999;18:282-290.

[25] Abramzon B, Sirignano WA. Droplet vaporization model for spray combustion calculations. Int J Heat Mass Transf 1989;32:1605-1618.

[26] Le Clercq PC, Bellan J. Direct numerical simulation of a transitional temporal mixing layer laden with multicomponent-fuel evaporating drops using continuous thermodynamics. Phys Fluids 2004;16:1884-1907.

[27] Kitano T, Nishio J, Kurose R, Komori S. Effects of ambient pressure, gas temperature and combustion reaction on droplet evaporation. Combust Flame 2014;161:551-564.

[28] Miller RS, Bellan J. Direct numerical simulation of a confined three-dimensional gas mixing layer with one evaporating hydrocarbon-droplet-laden stream. J Fluid

Mech 1999;384:293-338.

[29] Miller RS, Harstad K, Bellan J. Evaluation of equilibrium and non-equilibrium evaporation models for many-droplet gas-liquid flow simulations. Int J Multiph Flow 1998;24:1025-1055.

[30] Nomura H, Ujiie Y. Experimental study on high-pressure droplet evaporation using microgravity conditions. Proc Combust Inst 1996;26:1267-1273.

[31] Wang C, Dean AM, Zhu H, Kee RJ. The effects of multicomponent fuel droplet evaporation on the kinetics of strained opposed-flow diffusion flames. Combust. Flame 2013;160:265-275.

[32] Watanabe H, Matsushita Y, Aoki H, Miura T. Numerical simulation of emulsified fuel spray combustion with puffing and micro-explosion. Combust Flame 2010;157:839-852.

[33] Sato K. Estimation of physical property coefficients. Maruzen Publishing Co Ltd Japan 1954 (In Japanese).

[34] Honnet S, Seshadri K, Niemann U, Peters N. A surrogate fuel for kerosene. Proc Combust Inst 2009;32:485-492.

[35] Blanquart G, Pepiot-Desjardins P, Pitsch H. Chemical mechanism for high temperature combustion of engine relevant fuels with emphasis on soot precursors. Combust Flame 2009;156:588-607.

[36] Narayanaswamy K, Blanquart G, Pitsch H. A consistent chemical mechanism for oxidation of substituted aromatic species. Combust Flame 2010;157:1879-1898.

[37] Watanabe H, Kurose R, Hayashi M, Kitano T, Komori S. Effects of ambient pressure and precursors on soot formation in spray flames. Adv Powder Tech, accepted, doi:10.1016/j.apt.2014.03.022.

[38] Brown PN, Byrne GD, Hindmarsh AC. VODE: A variable-coefficient ODE solver. SIAM J Sci Stat Comp 1989;10:1038-1051.

[39] NIST 2011 http://webbook.nist.gov/chemistry/ In NIST Chemistry WebBook. NIST Standard Reference Database (ed. Linstrom PF, Mallard WG)

[40] Kee RJ, Dixon-Lewis G, Warnaz J, Coltrin ME, Miller JA. A fortran computer code package for the evaluation of gas-phase, multicomponent transport proper-

ties. Sandia Rep 1986;SAND86-8246.

[41] Kee RJ, Rupley FM, Miller JA. CHEMKIN-II: A fortran chemical kinetics package for the analysis of gas-phase chemical kinetics. Sandia Rep 1989;SAND89-8009B.

NOMENCLATURE

B_M	mass transfer number , -
c_p	heat capacity , J/(K kg)
D	diffusion coefficient , m^2/s
d	droplet diameter , m
L	Knudsen layer thickness , m
L_V	latent heat , J/kg
m	mass , kg
P	pressure , Pa
Pr	Prandtl number , -
R	universal gas constant , J/(K mol)
Re_{sl}	slip Reynolds number , -
Sc	Schmit number , -
Sh	Sherwood number , -
T	temperature , K
W	mole weight , g/mol
X	mole fraction , -
Y	mass fraction , -
ϵ	partial evaporation rate , -
μ	viscosity , Pa s
ρ	density , kg/m^3
τ	particle response time , s
0	initial value
avg	averaged
c	at critical point
d	droplet's
k	kth species
nb	at normal boiling point
s	at droplet surface
sat	saturated
V	vapor's

Table 1: Computational conditions.

Cases	P [MPa]	d_0 [μm]	Ambient gas	Fuel
Case 1	0.1	15.0	nitrogen	one-component fuel
Case 2	0.1	15.0	nitrogen	two-component fuel
Case 3	0.1	15.0	nitrogen	three-component fuel
Case 4	0.1	15.0	air	one-component fuel
Case 5	0.1	15.0	air	two-component fuel
Case 6	0.1	15.0	air	three-component fuel
Case 7	1.0	15.0	air	one-component fuel
Case 8	1.0	15.0	air	two-component fuel
Case 9	1.0	15.0	air	three-component fuel
Case 10	0.1	7.5	air	one-component fuel
Case 11	0.1	7.5	air	two-component fuel
Case 12	0.1	7.5	air	three-component fuel

Table 2: Physical properties.

Components	T_c [K]	T_{nb} [K]	$L_{V,nb}$ [kJ/kg]	c_p [J/(K kg)]	ρ [kg/m^3]	W [g/mol]
n-decane	619.0	447.3	279.7	2199.8	724.7	142.3
n-heptane	540.0	371.6	317.1	2232.5	679.4	100.2
1,2,4-trimethyl-benzene	654.7	442.6	398.8	1773.0	872.2	120.2
n-dodecane	658.2	489.0	256.5	2218.3	744.4	170.3
iso-octane	543.9	372.4	269.5	2045.9	690.0	114.2
toluene	593.0	383.8	360.1	1707.0	860.51	92.1

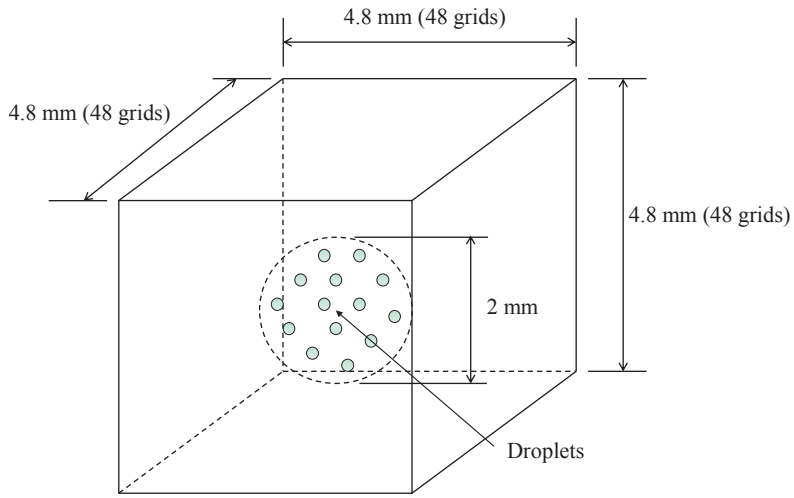

Figure 1: Computational domain.

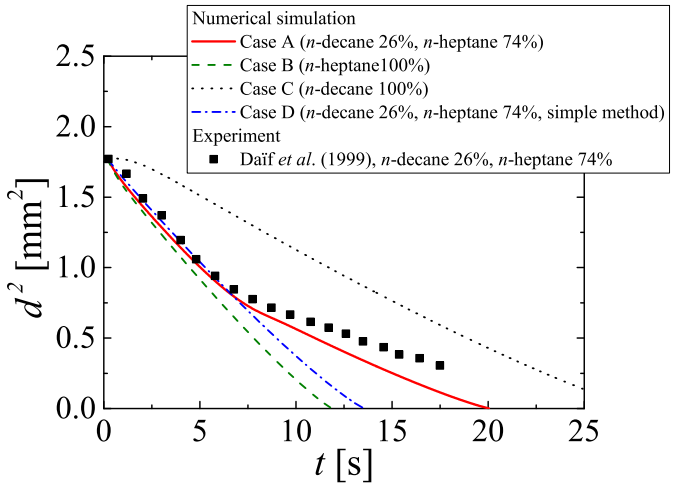

Figure 2: Comparison of predicted time variations of squared droplet diameter with experiment.

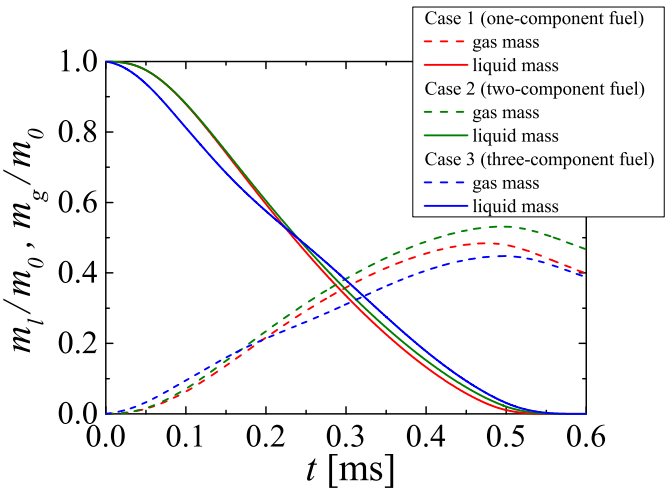

Figure 3: Time variations of normalized masses of gas and liquid fuels in nitrogen for P=0.1 MPa and d_0=15.0 μm for one-, two- and three-component fuels (Cases 1-3).

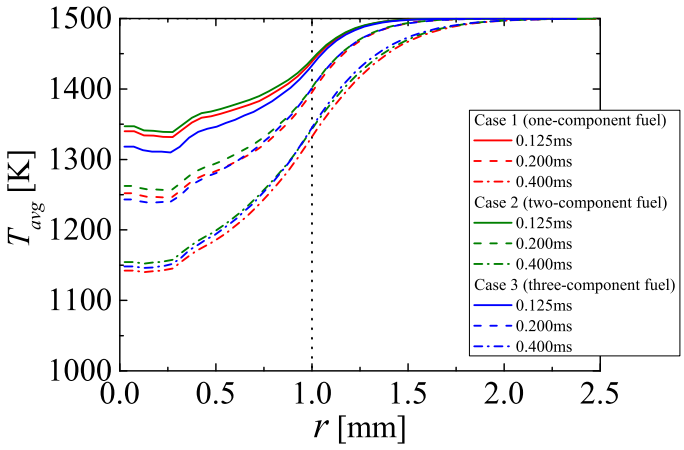

Figure 4: Radial distributions of spatial-averaged gas temperatures in nitrogen for P=0.1 MPa and d_0=15.0 μm for one-, two- and three-component fuels (Cases 1-3).

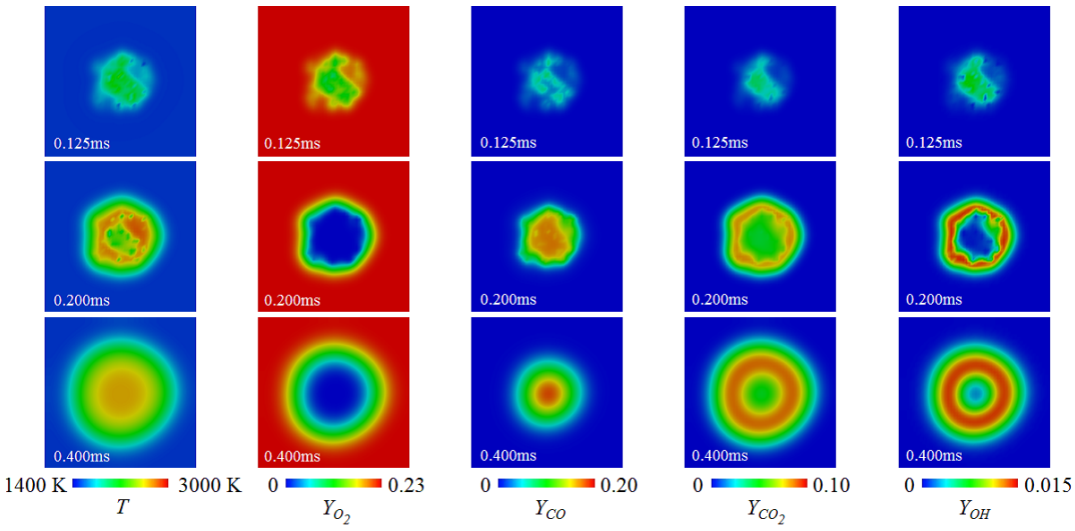

Figure 5: Instantaneous distributions of gas temperature, and mass fractions of O_2, CO, CO_2 and OH in air for P=0.1 MPa and d_0=15.0 μm at t=0.125 ms, t=0.200 ms and t=0.400 ms for a one-component fuel (Case 4).

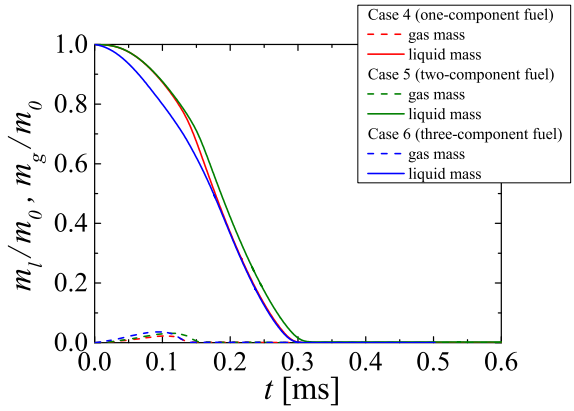

(a) P=0.1 MPa and d_0=15.0 μm (Cases 4-6)

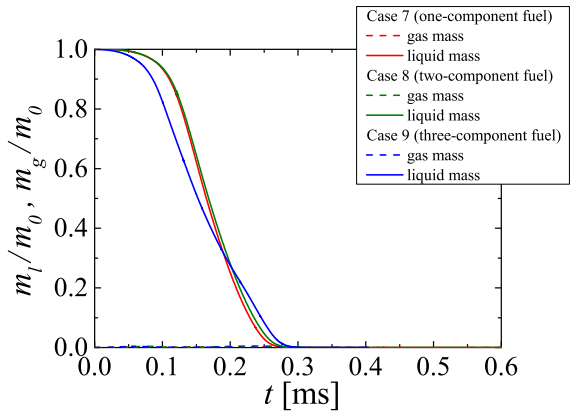

(b) P=1.0 MPa and d_0=15.0 μm (Cases 7-9)

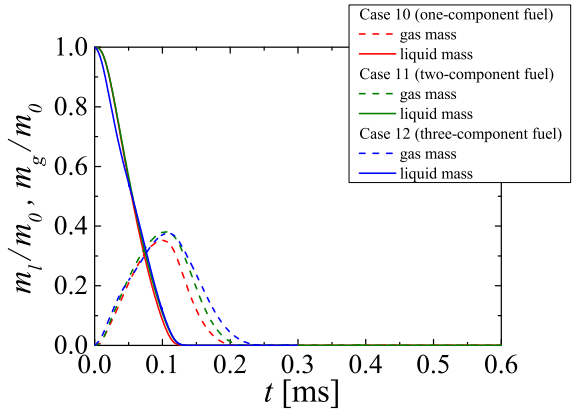

(c) P=0.1 MPa and d_0=7.5 μm (Cases 10-12)

Figure 6: Time variations of normalized masses of gas and liquid fuels in air for one-, two- and three-component fuels for (a) P=0.1 MPa and d_0=15.0 μm (Cases 4-6), (b) P=1.0 MPa and d_0=15.0 μm (Cases 7-9) and (c) P=0.1 MPa and d_0=7.5 μm (Cases 10-12).

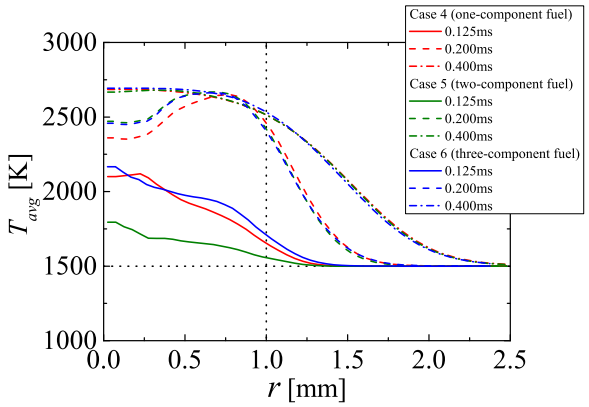

(a) P=0.1 MPa and d_0=15.0 μm (Cases 4-6)

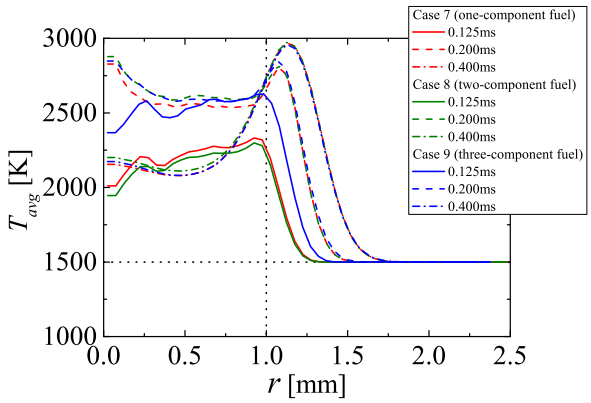

(b) P=1.0 MPa and d_0=15.0 μm (Cases 7-9)

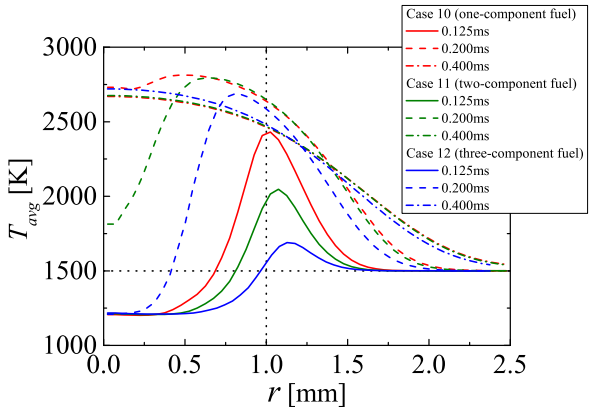

(c) P=0.1 MPa and d_0=7.5 μm (Cases 10-12)

Figure 7: Radial distributions of spatial-averaged gas temperatures in air for one-, two- and three-component fuels for (a) P=0.1 MPa and d_0=15.0 μm (Cases 4-6), (b) P=1.0 MPa and d_0=15.0 μm (Cases 7-9) and (c) P=0.1 MPa and d_0=7.5 μm (Cases 10-12).